JCTC Journal of Chemical Theory and Computation

Effects of Long-Range Electrostatics on Time-Dependent Stokes Shift Calculations

Kristina E. Furse and Steven A. Corcelli*

Department of Chemistry and Biochemistry, 251 Nieuwland Science Hall, University of Notre Dame, Notre Dame, Indiana 46556

Received March 25, 2009

Abstract: Molecular dynamics simulations are essential to the correct interpretation of the response measured in time-dependent Stokes shift (TDSS) experiments of fluorescent probe molecules in biological environments. Within linear response theory, the TDSS response is the time correlation function of the fluctuations of $\Delta E(t)$, the difference between the solute environment interaction energy with the probe, modeled in both its electronically excited and ground states. $\Delta E(t)$ is dominated by electrostatic interactions between the environment and the ground- and excited-state charge distributions of the probe. The treatment of the long-ranged electrostatics in the calculation of the TDSS response in MD simulations is systematically investigated for three probes in aqueous solution: a model diatomic, coumarin 102, and Hoechst 33258. Nine different protocols for the treatment of the electrostatics were compared to particle mesh Ewald (PME), which was utilized as a reference standard. A computationally efficient pairwise alternative to PME, the damped shifted force method, was shown to reproduce the TDSS response calculated with PME for all three systems. In contrast, neglecting the role of the long-ranged electrostatics in the calculation of the TDSS response results in artifacts.

I. Introduction

There is currently great interest in using computational methods to interpret solvation dynamics experiments of fluorescent probe molecules in heterogeneous or confined environments.[1−9] The typical practice is to collect an equilibrium MD simulation with the probe of interest modeled in its ground electronic state and then to postprocess the trajectory to calculate the solvation response, which describes the dynamics of the environment in the vicinity of the probe. Since the solvation response is generally short-ranged and is usually dominated by atoms within ∼5 Å of the probe,[4,10−12] it is not clear what role, if any, the handling of long-range electrostatics plays in computing the solvation response.

The complete electrostatic potential energy for a periodic system is the sum of the Coulomb interactions between all pairs of atomic partial charges, including their periodic replicas. Without further approximation, the direct calculation of this infinite sum is computationally intractable. An obvious approach is the introduction of a spherical cutoff in which the Coulombic interactions are only calculated between pairs of charges whose spatial separation is less than a specified distance. However, this strategy fails because the electrostatic sum is conditionally convergent; the value of the sum as a function of the cutoff distance will not converge unless the portion of the system within the cutoff sphere is charge neutral, which is not generally the case. Moreover, cutoffs introduce a discontinuity into the energy and forces, which have some finite value within the cutoff radius that immediately drops to zero outside of the radius, leading to instabilities in simulations as atoms cross the boundary. Improper handling of interactions at a cutoff boundary can cause serious artifacts that dramatically affect the accuracy of calculations.

A number of different methods to handle long-range electrostatics have been developed that circumvent the difficulties posed by the conditional convergence of the electrostatic sum,[13−15] including Ewald summation,[16−19] implicit continuum dielectric,[20,21] and fast multipole or reaction field approaches.[14,19,22] In addition, for systems

* Corresponding author. E-mail: scorcell@nd.edu.

10.1021/ct9001416 CCC: $40.75
Published on Web 07/23/2009

containing explicit dipoles, an explicit real-space lattice summation method has been developed by Ladd[23,24] and applied to the calculation of static- and frequency- dependent dielectric constants[25,26] as well as in the context of solvation dynamics.[27] Each of these methods has strengths and weaknesses that strike a different balance between physical accuracy and computational cost. Currently, the accepted methodology for the MD simulation of biomolecular systems is to treat the long-range electrostatics with an Ewald summation method, typically a computationally efficient variation called particle mesh Ewald (PME).[16,17] The Ewald summation methods involve a division of the electrostatic sum into two absolutely convergent components: a real-space sum, representing the atoms within a specified cutoff radius, and a long-ranged reciprocal-space sum. While Ewald summation methods have proven to be extremely accurate, they are not ideal for postprocessing trajectories to calculate the solvation response for several reasons. First, they are nontrivial to implement when developing new methods, and they become computationally expensive for large systems. Most importantly, it is not clear how to decompose the collective solvation response to distinguish individual contributions in multicomponent systems, which represents a significant theoretical limitation.

Ideally, an electrostatics method for solvation dynamics calculations would involve a direct pairwise sum with minimal modifications to eliminate cutoff artifacts. One compelling option is based on two key observations described by Wolf et al.[28] First, electrostatic interactions are *effectively* short-ranged in condensed-phase systems. Therefore, for the larger boxes typical of modern biomolecular simulation with a proper treatment of the electrostatic sum, convergence can be achieved within the central unit cell and does not require inclusion of explicit periodic images. The second key observation is the critical importance of neutralization of charge within the cutoff radius, which renders the electrostatic sum absolutely convergent. This neutralization is achieved mathematically by shifting the Coulomb potential so that it effectively goes to zero at the cutoff radius. This operation also has the advantage of eliminating the discontinuities in the energies at the cutoff radius. The physical interpretation of this mathematical shift is a projection of image charges equal and opposite to the charges within the cutoff onto the cutoff sphere, achieving charge neutralization within the spherical cutoff surface.

Fennell and Gezelter[29] have extended and refined this pairwise alternative to the Ewald summation methods[28−30] and extensively validated two variations of the shifted potentials against PME. MD simulations were conducted using seven different test systems, spanning a range from neutral liquids to ionic crystals. One of the new pairwise methods, damped shifted force (DSF), emerged as superior, accurately reproducing the energetic and dynamic results computed with PME. In addition to shifting the Coulomb potential to zero at the cutoff radius, DSF also shifts the Coulombic forces to zero at the cutoff, thereby incorporating the same image charges into the force calculation as well as eliminating discontinuities in the forces. The DSF method is also versatile; while it is fully appropriate for systems with three-dimensional periodicity, it does not actually require periodic images so it can also be used for nonperiodic systems and for those with two-dimensional periodicity. The major advantage for postprocessing trajectories to calculate the solvation response is that DSF involves a simple pairwise sum that can be rapidly calculated and trivially decomposed to isolate component contributions (e.g., solvent, counterions, and biomolecules).

In order to investigate systematically the effect of different electrostatics protocols on solvation dynamics calculations, we have chosen three probe/solvent systems of increasing complexity: (1) a neutral, rigid model diatomic molecule in water, (2) a neutral, flexible probe, coumarin 102 (C102), in water, and (3) a positively charged, flexible probe, Hoechst 33258 (H33258), in water with a single Cl^- counterion. The H33258[3,31] and C102[8,32−42] probes have been utilized for solvation dynamics studies of water at the DNA interface. After performing MD simulations for all three systems using the AMBER package with periodic boundary conditions and PME, we postprocessed each simulation using ten different solvation dynamics protocols that represent variations of three electrostatics methods: direct Coulombic sums, DSF, and PME as a reference standard. Because the strengths and weaknesses of the PME method have been extensively characterized in the literature,[43−48] it provides an ideal benchmark to evaluate the accuracy of the other treatments of the long-ranged electrostatics in the context of computing time-dependent Stokes shift (TDSS) responses. We found that the handling of electrostatics is extremely important, even with a cutoff radius three to four times larger than the probe range. Not surprisingly, bare Coulombic cutoffs lead to artifacts in the solvation dynamics calculations for all three test systems. Incorporation of a standard switching function and group-based imaging was sufficient to resolve the problems in the two neutral systems. However, these simple strategies were not sufficient to resolve unexpected artifacts in the most complex test system, H33258. This is an important cautionary note since the H33258 system with its mobile counterion is more representative of the complex, multicomponent biological systems being studied today. All of the artifacts disappeared with the DSF methods, which appear to be a simple and efficient alternative to Ewald summation for solvation dynamics calculations.

II. Computational and Theoretical Methods

A. Solvation Dynamics Calculations. The central quantity in computational studies of solvation dynamics is the instantaneous solvation energy, $\Delta E(t)$, which is the difference in the solute−solvent interaction energy with the solute modeled in both its excited and ground electronic states. According to linear response theory, the solvation response or time-dependent Stokes shift (TDSS), $S(t)$, is equal to the equilibrium time correlation of fluctuations in ΔE:[49,50]

$$S(t) \cong C_{0(1)}(t) = \frac{\langle \delta\Delta E(0)\delta\Delta E(t)\rangle_{0(1)}}{\langle |\delta\Delta E|^2\rangle_{0(1)}} \qquad (1)$$

Table 1. Abbreviations for Solvation Dynamics Methods

Ewald	particle mesh Ewald
DSF_00	damped shifted force, $\alpha = 0.0$ Å^{-1}
DSF_01	damped shifted force, $\alpha = 0.1$ Å^{-1}
DSF_02	damped shifted force, $\alpha = 0.2$ Å^{-1}
grpCut	pairwise Coulomb, group-based bare cutoff
grpCutSw	pairwise Coulomb, group-based cutoff with a switching function
grpNoCut	pairwise Coulomb, group-based imaging, no cutoff
atmCut	pairwise Coulomb, atom-based bare cutoff
atmCutSw	pairwise Coulomb, atom-based cutoff with a switching function
atmNoCut	pairwise Coulomb, atom-based imaging, no cutoff

where $\delta\Delta E(t) = \Delta E(t) - \langle \Delta E \rangle_{0(1)}$ and $\langle \cdots \rangle_{0(1)}$ indicates an ensemble average in the either the ground or excited electronic states of the solute.

For the present calculations, which are based on methodology developed in numerous previous MD studies of solvation dynamics,[4−7,27,49,51−68] it is assumed that the electronic excitation occurs so quickly that the geometry of the solute does not change (vertical transition). It is reasonable to model the transition classically as a redistribution of atomic partial charges. Within this description, $\Delta E(t)$ is easily computed for a given instantaneous configuration of the solvent as the difference in the solute−solvent electrostatic potential energy for the ground-state solute partial charges and for the excited-state partial charges, $\Delta E(t) = E_{\text{excited}}(t) - E_{\text{ground}}(t)$.[49]

Direct Pairwise Coulomb Methods. For N_{solute} charged sites interacting with N_{solvent} charged solvent sites, the energy difference $\Delta E(t)$ is typically calculated as a pairwise Coulomb sum:

$$\Delta E(t) = \sum_{i=1}^{N_{\text{solute}}} \Delta q_i \sum_{j=1}^{N_{\text{solvent}}} \frac{q_j}{r} \tag{2}$$

where Δq_i is the difference in partial charge ($q_{\text{excited}} - q_{\text{ground}}$) on solute site i, q_j is the partial charge on solvent atom j, and r is the interatomic separation between solute atom i and solvent atom j at time t. We have considered six different variations on this basic approach (Table 1). Three involve calculating r as the minimum distance of individual solvent atoms to solute atoms (atom-based imaging and cutoffs), and three involve considering the solvent as intact molecules (group-based imaging and cutoffs). In the latter approach, an entire water molecule was considered to be within the cutoff if the oxygen atom fell within the specified radius. The cutoffs used in the present work were set equal to one-half the box length, approximately 14, 15, and 20 Å for the diatomic, C102 and H33258 systems, respectively.

For both the atom- and group-based methods, we performed three different solvation dynamics calculations: (1) using a bare cutoff, applying eq 2 only to atoms (or molecules) within a specified radius from solute atoms, (2) using a switching function, scaling the electrostatic interaction with solvent near the cutoff to eliminate the discontinuities in the electrostatic potential energy and forces, and (3) no cutoff, applying eq 2 to the entire system (not including periodic images). All are standard protocols that have been used to handle electrostatics, although bare atom-based cutoffs have been largely phased out. We include them here for comparison since the DSF method utilizes atom-based imaging and cutoffs.

DSF. The cutoff neutralized damped shifted force (DSF) method is a variation on a simple pairwise Coulomb sum that eliminates artifacts that arise from truncating long-ranged electrostatic interactions with a cutoff, yielding results that are consistent with more complex Ewald summation methods.[28−30] Using the DSF formalism, $\Delta E(t)$ is expressed as

$$\Delta E(t) = \sum_{i=1}^{N_{\text{solute}}} \Delta q_i \sum_{j=1}^{N_{\text{solvent}}} q_j \left[\frac{\operatorname{erfc}(\alpha r)}{r} - \frac{\operatorname{erfc}(\alpha R_c)}{R_c} + \left(\frac{\operatorname{erfc}(\alpha R_c)}{R_c^2} + \frac{2\alpha}{\sqrt{\pi}} \frac{\exp(-\alpha^2 R_c^2)}{R_c} \right)(r - R_c) \right] \tag{3}$$

where Δq_i is the difference in partial charge ($q_{\text{excited}} - q_{\text{ground}}$) on solute site i, q_j is the partial charge on solvent atom j, r is the interatomic separation between solute atom i and solvent atom j at time t, and R_c is the cutoff radius ($r \le R_c$). The parameter α in the complementary error function controls the range of damping; its purpose is to accelerate convergence of the Coulombic sum. We evaluated three different values of α representing increasing degrees of damping: 0.0, 0.1, and 0.2 Å^{-1}. For all of the DSF calculations, simple atom-based imaging and cutoffs were used, analogous to atmCut. Preliminary tests confirmed that incorporating group-based imaging and/or switching functions had no significant effect on the DSF results.

Ewald Summation. For each trajectory frame, we calculated the energy of the entire system using the excited-state solute charges and the ground-state solute charges; their difference is $\Delta E(t)$. We used smaller cutoff radii for the Ewald summation solvation dynamics calculations since the cutoff simply represents the boundary between the real and reciprocal space terms: 10, 10, and 16 Å for the diatomic, C102 and H33258, respectively.

Component Contributions. For all three probe systems, the ΔE calculation methods sum the interaction energy of the solute with the water molecules within the cutoff, R_c (if present). For the simple diatomic probe, water is the only environmental component, $\Delta E = \Delta E_{\text{water}}$. For the two flexible fluorescent probes, C102 and H33258 (Figure 1), ΔE also includes the interaction of the solute with itself via the electrostatic terms in the solute intramolecular molecular mechanics potential energy. For the "self-solvation" component of ΔE, we adopted standard handling of the intramolecular electrostatic energy: nonbonded pair lists were generated for each solute atom so that 1−1, 1−2, and 1−3 interactions are ignored, and 1−4 interactions are scaled down by a factor of 1.2. In this notation, the numbers correspond to relative solute atom positions: 1−1 refers to interaction of an atom with itself, 1−2 refers to interaction of an atom with its bonded neighbors, 1−3 refers to interaction of an atom with atoms exactly 2 bonds away, and so on. These interactions are described by the bond, angle, and torsion terms in the force field, so the electrostatics term is eliminated or scaled.

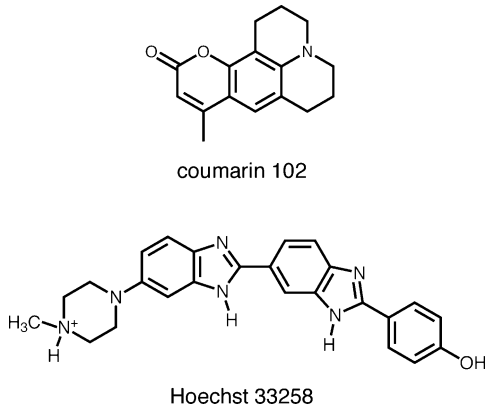

Figure 1. Structures of the fluorescent probes coumarin 102 and Hoechst 33258. The latter has a net charge of +1 due to the protonated piperazine group.

Since ΔE is calculated as a simple pairwise electrostatic sum in eqs 1 and 2, the results of the pairwise Coulombic and DSF solvation dynamics methods can be trivially decomposed into individual component contributions. For the C102 system, the instantaneous solvation energy has two components, water and solute conformation, $\Delta E = \Delta E_{\text{water}} + \Delta E_{\text{conf}}$. The positively charged H33258 system contains one additional component, the chloride counterion, $\Delta E = \Delta E_{\text{water}} + \Delta E_{\text{conf}} + \Delta E_{\text{ion}}$. Solvation response functions for each individual environmental component can be calculated by decomposing $C(t)$ into partial correlation functions:[4,6]

$$C^{\alpha}_{0(1)}(t) = \frac{\langle \Delta E_{\alpha}(t)\Delta E(0)\rangle_{0(1)} - \langle \Delta E_{\alpha}\rangle_{0(1)}\langle \Delta E\rangle_{0(1)}}{\langle \Delta E(0)\Delta E(0)\rangle_{0(1)} - \langle \Delta E\rangle_{0(1)}\langle \Delta E\rangle_{0(1)}} \quad (4)$$

Decomposing the reciprocal space portion of the Ewald sum into component contributions is conceptually less straightforward and was not attempted here. In the absence of Ewald results, the full direct Coulomb sum with group-based imaging and no cutoff (grpNoCut) was used as a reference standard to evaluate the decompositions.

B. Parameter Development. The solutes studied here are not well represented by parameters available in the standard AMBER ff99 force field,[69] so new parameters were developed, including the creation of new atom types. As discussed in Section II-A, the atomic partial charges of the solute in its ground and excited electronic states are essential for computing solvation response functions. Force field parameters for the ground and excited states of all three probes were generated as follows.

Diatomic. The atoms of the diatomic molecule were given radii of 1.66 Å, a rigid bond length of 1.25 Å, and ground-state charges of 0 (similar to standard models of molecular oxygen). The hypothetical "excited state" was modeled with charges of +0.5 and −0.5 on the two atoms to create an instant dipole but maintain overall charge neutrality.

Coumarin 102. Coumarins are extremely well-studied fluorescent probes, so much of the structural and electronic information needed to calculate the missing force field parameters was available in the literature. The gas-phase minimum energy structure for C102, computed with density functional theory with the B3LYP[70−72] functional and a 6-311G(d,p) basis set, was taken from Cave and Castner.[73] We took missing equilibrium bond lengths and angles from this minimum energy structure and interpolated the force constants using reference values in the ff99 force field.[69] The new equilibrium angles were adjusted to fit with existing ff99 parameters so that the interior angles of planar rings summed to the appropriate values (e.g., 720° for 6-membered rings). We set missing dihedral and improper torsion parameters equal to existing ff99 parameters that describe structurally similar rings found in amino and nucleic acids.

For the ground state, we calculated a molecular electrostatic potential over a grid of points using the optimized geometry and HF/6-311+G(d,p) basis set. We then fit the electrostatic potential to an atom-centered point charge model according to the RESP procedure.[74] Charges on topologically equivalent atoms were subsequently averaged (equivalenced) as in the standard AMBER charge fitting protocol. Basic CIS/6-31G(d) calculations proved insufficient to describe the excited state, giving no change in dipole moment. Ingrosso et al. calculated ground- and excited-state atomic charges for C153, which differs from C102 by a trifluoromethyl group and used them successfully to study solvation dynamics in acetonitrile.[55] C102 and C153 have similar spectral properties, including a similar change in dipole moment upon excitation.[73] We applied the atomic charge differences ($\Delta q = q_{\text{excited}} - q_{\text{ground}}$) from the C153 work to our ground-state charges to generate excited-state charges for C102. Classical dipole moment calculations on the resulting charge distributions using AMBER revealed that they were reasonable, giving an increase of 3.1 D upon excitation ($\mu_{\text{excited}} = 10.2$ D, $\mu_{\text{ground}} = 7.1$ D), which is consistent with the increase of 2.0 D ($\mu_{\text{excited}} = 9.2$ D, $\mu_{\text{ground}} = 7.2$ D) from other ab initio calculations on C102[73] as well as the range of values, 2.1−3.8 D, from microwave and solvatochromism experiments.[75,76] All new C102 force field parameters, including charges, are included as Supporting Information.

Hoechst 33258. The fluorescent probe H33258, 2′-(4-hydroxyphenyl)-5-(4-methyl-1-piperazinyl)-2,5′-bibenzimidazole (Figure 1), is comprised of four structural units connected by three torsion angles (α, β, and γ), which are the key determinants of its conformation. It has greater inherent conformational flexibility than coumarin and required many ab initio calculations, including multiple torsion angle potential energy scans to describe its motion. It also exhibits more complex spectroscopy, including evidence of significant structural changes upon excitation, and proton transfer and rotation about the bisbenzimide axis, depending on pH and degree of confinement.[31,77] The procedures we used to develop H33258 parameters are described in detail elsewhere, and the parameters are included as Supporting Information in that paper.[10]

C. Molecular Dynamics Simulations. MD simulations were performed using AMBER 9.0[78] with the AMBER ff99 force field[69] and the SPC/E water model.[79] The diatomic molecule and geometry-optimized conformations of C102 and H33258 were solvated in cubic periodic boxes with a minimum buffer of 10 Å from any solute atom to the closest box edge. A chloride counterion was added to the H33258 simulation to establish charge neutrality. The final unit cells were (1) diatomic with 673 water molecules: 2 021 total

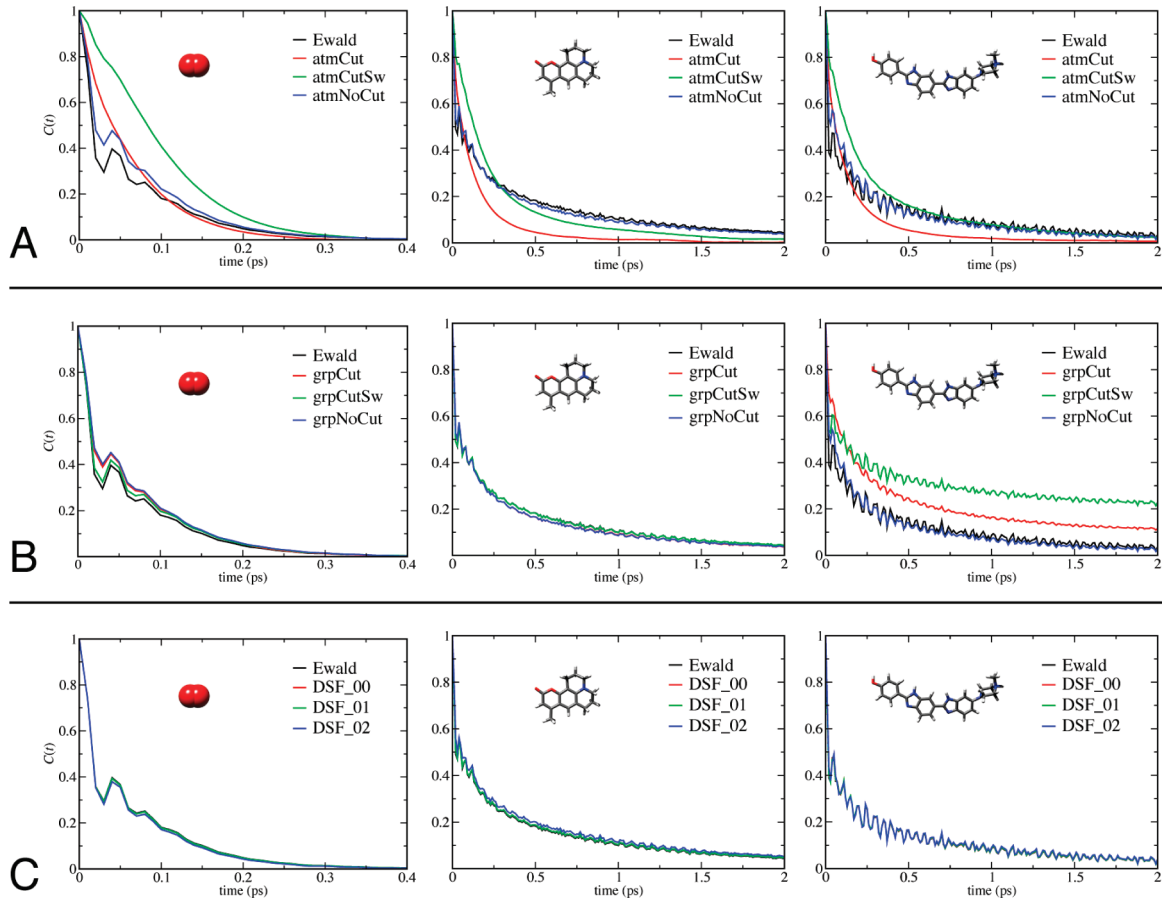

Figure 2. Comparison of time-dependent Stokes shift calculations using 10 different variations of direct Coulomb and DSF electrostatics methods. PME results (black curves) are included as a reference standard. Row A, direct Coulomb methods with atom-based imaging. Row B, direct Coulomb methods with group-based imaging. Row C, DSF methods. Each column represents a different solute in water: diatomic molecule, coumarin 102, and Hoechst 33258 with a Cl^- counterion.

atoms, (2) C102 with 973 water molecules: 2 955 total atoms, and (3) H33258 with Cl^- and 2 325 water molecules: 7 033 total atoms.

The same equilibration procedure was used for all three systems and is described in detail elsewhere.[10] Production MD trajectories were performed in the NVE ensemble with the H33258 and C102 molecules fully flexible except for all covalent bonds containing hydrogen, which were fixed at equilibrium lengths using the SHAKE algorithm.[80] The diatomic was held rigid but could translate and rotate in the box, as could the fluorescent probes. A 2 fs integration time step was used, and configurations were collected every 10 fs for subsequent analysis. A PME summation method was used to compute long-range electrostatic energy and force corrections[16] with a 9 Å real-space nonbonded cutoff. The data collection phase consisted of one 10 ns trajectory for the diatomic, four 6 ns trajectories (24 ns) for C102, and seven 1.5−6 ns trajectories (22.5 ns) for H33258.

III. Results and Discussion

A. Collective TDSS. Figure 2 shows the collective TDSS curves for all three test systems, using each of the nine pairwise electrostatics methods, compared to reference curves calculated with PME (black). Previous multiexponential fits to the H33258 DSF_02 data yielded time scales for the solvation response of H33258 free in aqueous solution (0.17 and 1.4 ps)[10] and bound to DNA (1.5 and 20 ps)[3] that were highly consistent with the results of ultrafast fluorescence experiments (0.2 and 1.2 ps, 1.4 and 19 ps, respectively),[31] validating our simulations and general solvation dynamics methodology.

The TDSS curves generated with the DSF methods (Figure 2, row C) are nearly indistinguishable from the Ewald results for all three systems. Variation in the degree of dampening (alpha = 0.0, 0.1 or 0.2) has little to no effect except for the C102 system, where the curve deviates slightly when alpha = 0.2, suggesting minor overdamping. Motion of the solute itself (internal conformational changes, not overall translation and rotation) contributes oscillations that are proportional to the degree of solute flexibility.[10] Internal motion of the C102 probe imparts minor oscillations and is responsible for a small portion (~3%) of the solvation response. Motion of the flexible H33258, which has four subunits that can rotate relative to one another, contributes more significant oscillations and is responsible for approximately one-third of the total solvation response. However, the short-lived oscillations in the computed rigid diatomic solvation response must have a different origin because there is no conformational freedom. Similar oscillations have been reported in numerous other studies of atomic and diatomic probes and have been attributed to coherent vibration of the solvation shell, an effect that is damped and far more subtle with polyatomic

probes.[58,81] Interestingly, recent experimental studies indicate the presence of both types of oscillations for a quinolone probe: high-frequency oscillations corresponding to probe intramolecular motion in addition to a broader 170 fs oscillation feature attributed to coherent water motion.[82] Related work in acetonitrile showed oscillations associated with solvent librational motion for certain nitrofluorenes but not for C153.[83] This is consistent with our simulations of the TDSS of C102 in water, which showed minor oscillations due to probe conformation but not coherent solvent motion. All of this suggests that the fast oscillatory components of the solvation response represent a complex interplay of probe and solvent structure and dynamics and warrant more study.

The results for the six direct Coulomb sum methods are much more variable than the DSF results. Atom-based imaging (with or without a switching function) shows the largest deviations from Ewald, giving featureless curves that exhibit the wrong time scales (Figure 2, row A). Reasonable accuracy is only recovered when the full interaction is calculated (atmNoCut), and even then the TDSS curves for the diatomic and H33258 systems deviate from the Ewald standard at early times. The DSF method also utilizes atom-based cutoffs, but the force shifting eliminates the artifacts seen with these direct Coulomb sums.

Group-based imaging is more robust, giving reasonable accuracy for the two neutral systems, the diatomic and C102 (Figure 2, row B). Interestingly, with group-based imaging, the TDSS curve calculated, using a cutoff with switching function (grpCutSw), is more consistent with Ewald than with that of the full interaction (grpNoCut). However, group-based imaging breaks down dramatically for the more complex H33258 system. The TDSS curves exhibit a long-time component and do not approach zero within 5 ps like the Ewald curve. This offset, which is even more pronounced when a switching function is added (grpCutSw), could be mistakenly interpreted as slow molecular motion in the system. Decomposition of the collective TDSS associated the long time component with movement of the ion across the cutoff boundary (see Supporting Information). The origin of this artifact in the H33258 system is explored further in the following section (Section III B).

B. H33258: Component Contributions. There are two primary factors that lead to the differences in the TDSS curves for the H33258 system (Figure 2, column 3): the fluctuation patterns of the solvent and ion components of the instantaneous solvation energy (ΔE_{water} and ΔE_{ion}) and their relative magnitudes. Since H33258 was always fully contained within the cutoff boundaries, the solute conformation (ΔE_{conf}) did not contribute to the observed differences and will not be considered here.

Atom-based cutoffs, which truncate solvent molecules at the cutoff radius, lead to dramatic overestimation of the solvent fluctuations (Figure 3, row A). Addition of a switching function reduces the fluctuations by an order of magnitude but does not completely resolve the problem. Calculating the full interaction (atmNoCut) restores the balance between the solvent and ion components, revealing important details like the inverse relationship between the two fluctuation patterns: as the ion contribution increases in magnitude, the solvent contribution decreases. This relationship has been discussed in other computational studies.[7]

Keeping solvent molecules intact with group-based cutoffs eliminates the wild solvent fluctuations, but reveals a more subtle issue with the ion component (Figure 3, row B). As the ion moves away from the solute, its contribution to the instantaneous solvation energy should decrease in magnitude. When a bare cutoff is used, the interaction between the solute atoms and the ion instantly go to zero one by one: the ion passes out of range of the solute atoms that are farthest away, while it remains within the cutoff of nearer solute atoms. As a result, the ion sees a varying subset of the total change in solute charge distribution (which is no longer net neutral) as it moves across the cutoff, causing severe fluctuations in interaction energy where there should be a gradual decline (compare left and right panels of Figure 3, row B). Addition of a switching function reduces the magnitude of these spurious fluctuations but does not correct the fluctuation pattern, and therefore, still leads to an inaccurate TDSS. In fact, the false long-time component in the TDSS curve is even more pronounced (Figure 2, row B). Since the ion is monatomic, ΔE_{ion} is identical whether the cutoff is atom- or group-based, but with atom-based cutoffs, the anomalous behavior is masked by the solvent fluctuations and does not cause a long-time offset in the TDSS profile.

Although the DSF method utilizes an atom-based cutoff, it does not exhibit the same fluctuation artifacts seen with bare cutoffs and simple switching functions (Figure 3, row C). The solvent and ion fluctuation patterns for the DSF method are similar to the direct Coulomb sum with no cutoff, yielding similar TDSS profiles. The one caveat with the DSF methods is the slight reduction in the magnitude of the fluctuations compared to the results for the full interaction, proportional to the degree of damping. Since the reduction affects both solvent and ion components, the balance between components is maintained, but care should be taken with any calculation that involves the absolute magnitude of the fluctuations (Section III C).

C. Static Stokes Shift. In addition to the dynamic aspects of the solvation response, researchers are also interested in calculating the magnitude of the static Stokes shift. We calculated the static Stokes shift for each of the systems with all 10 long-range electrostatics methods (Table 2). The large variation in the magnitude of fluctuations in ΔE for the direct Coulomb methods (Figure 3) leads to a broad range of estimates of the static Stokes shift. Bare atom-based cutoffs are the worst, overestimating the static Stokes shift by 500- to 2 500-fold. Switching functions and group-based cutoffs reduce the estimates significantly but do not completely alleviate the problem. Even when no cutoff is used, the static Stokes shift is still overestimated compared to Ewald summation. In contrast, the DSF methods give results for the static Stokes shift that are most similar to the Ewald benchmarks. For example, with a damping parameter of 0.1 $Å^{-1}$, DSF produced static Stokes shifts that were in error by just 3.3, 1.8, and 7.5% for the model diatomic, C102, and H33258 in aqueous solution, respectively.

To lend perspective to the comparisons in Table 2, we have included experimental estimates of the static Stokes

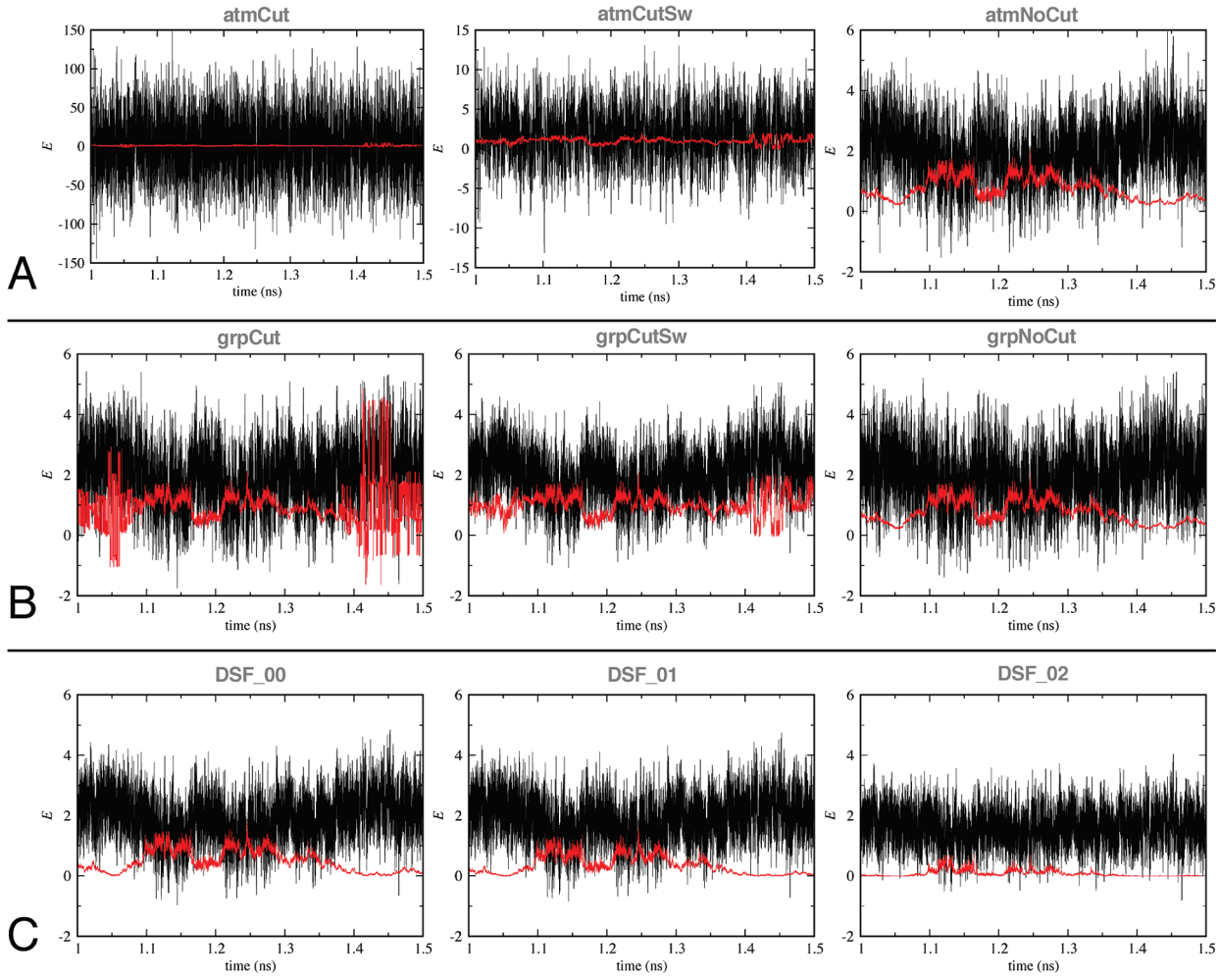

Figure 3. Individual solvent (black) and ion (red) contributions to the instantaneous solvation response, $\Delta E_{water}(t)$ and $\Delta E_{ion}(t)$ in kcal/mol, calculated for simulations of the fluorescent dye Hoechst 33258 in water with a Cl^- counterion. Each plot represents solvation dynamics results using a different electrostatics method: Row A, direct Coulomb with atom-based imaging: bare cutoff (left), switching function (center), and no cutoff (right). Row B, direct Coulomb with group-based imaging: bare cutoff (left), switching function (center), and no cutoff (right). Row C, DSF: $\alpha = 0.0$ (left), $\alpha = 0.1$ (center), and $\alpha = 0.2$ (right).

Table 2. Static Stokes Shift Comparison[a]

method	diatomic	C102	H33258
Ewald	9.0	6.0	0.80
DSF_00	8.5	5.5	0.75
DSF_01	8.7	5.7	0.74
DSF_02	8.0	4.2	0.58
grpCut	12.5	7.2	2.43
grpCutSw	9.7	6.3	1.10
grpNoCut	13.1	7.4	1.28
atmCut	6 622	2 669	1 799
atmCutSw	425	109	13.99
atmNoCut	12.1	7.2	1.17
experiment	–	5.6[84]	9.1[31]

[a] $\Delta\Delta E = (\langle|\delta\Delta E|^2\rangle_0)/k_BT$, results given in kcal/mol.

shift for C102[84] and H33258[31] in water. Since C102 is only sparingly soluble in water, our result is a prediction, and the experimental result is shown for a related coumarin molecule, C343. Cave and Castner[73] have established that these molecules (C102 and C343) have almost identical spectral properties, including a similar change in dipole moment upon electronic excitation. Therefore, C102 would be expected to have a similar static Stokes shift as C343. Our Ewald, DSF and grpCutSw calculations are all consistent with the experimental results for C102 but significantly underestimate the shift for H33258. To elucidate the origin of this discrepancy, it is important to emphasize the intrinsic difficulties associated with accurate computations of the static Stokes shift using the same classical models that are successful in computing the TDSS. Obtaining an accurate static Stokes shift requires knowledge of the average ground and excited electronic charge distribution of the solute molecules in their condensed-phase environment. However, in modeling these systems classically, the required charge distributions were calculated using quantum chemical calculations performed with the solute molecules in the gas phase. Owing to linear response theory, the TDSS, which is primarily dictated by solvent properties and the overall spatial variation the in the electric field the solvent experiences upon charge rearrangement in the solute,[58,81] is robust with respect to the overall accuracy of the ground- and excited-state charge distributions. For example, despite the inaccuracy of the static Stokes shift for H33258 in water, the computed time scales for the TDSS in aqueous solution (0.17 and 1.4 ps)[10] and bound to DNA (1.5 and 20 ps)[3] are in excellent

agreement with experiment (0.2 and 1.2 ps, 1.4 and 19 ps, respectively).[31] It is a success that the DSF computed static Stokes shifts are in agreement with the Ewald benchmarks, even if the agreement with experiment is inadequate. MD calculations of more accurate static Stokes shifts will require continued advances in electronic structure that yield accurate excited-state charge distributions in the condensed phase.

IV. Summary and Conclusions

In this work, we have studied three systems of increasing complexity to determine the effect of different electrostatics methods on solvation dynamics calculations. While it is generally true that the solvation response is dominated by atoms within ~5 Å of the probe, we have found that improper handling of long-range electrostatics and cutoffs can introduce serious artifacts that could lead to misinterpretation of solvation dynamics calculations. For neutral systems with homogeneous solvent, a simple direct Coulomb sum with a group-based cutoff and switching function was sufficient to achieve reasonably accurate results for both the TDSS and the static Stokes shift. However, for the charged solute with a mobile counterion, this method broke down, giving an artificial long-time component. Our results suggest that for more complex, multicomponent systems with mobile charged groups, a method such as DSF or Ewald should be used to eliminate cutoff artifacts and address long-range electrostatics.

DSF has several important advantages over Ewald-based methods for these types of calculations, including ease of implementation, speed, and trivial decomposition into component contributions. If the research question relates to dynamic properties, such as the TDSS, then DSF methods rival Ewald in terms of accuracy for a fraction of the cost. The one potential disadvantage of DSF-based methods is that excessive damping reduces the magnitude of fluctuations in the instantaneous solvation energy, leading to an underestimation of the static Stokes shift. Careful choice of a damping parameter can minimize this reduction. DSF gave results for the static and dynamics Stokes shift that were the most consistent with Ewald of all of the systems studied here.

Acknowledgment. SAC gratefully acknowledges the support of the National Science Foundation (CHE-0845736), the Northwest Indiana Computational Grid, and the Notre Dame Center for Research Computing. The authors also thank Professor J. Daniel Gezelter and Dr. Charles F. Vardeman II for helpful discussions.

Supporting Information Available: Component decomposition of the TDSS for H33258 and molecular dynamics force field parameters for ground and excited state coumarin 102 are included. This material is available free of charge via the Internet at http://pubs.acs.org.

References

(1) Faeder, J.; Ladanyi, B. M. *J. Phys. Chem. B* **2001**, *105*, 11148.

(2) Feng, X. B.; Thompson, W. H. *J. Phys. Chem. C* **2007**, *111*, 18060.

(3) Furse, K. E.; Corcelli, S. A. *J. Am. Chem. Soc.* **2008**, *130*, 13103.

(4) Golosov, A. A.; Karplus, M. *J. Phys. Chem. B* **2007**, *111*, 1482.

(5) Li, T. P.; Hassanali, A. A. P.; Kao, Y. T.; Zhong, D. P.; Singer, S. J. *J. Am. Chem. Soc.* **2007**, *129*, 3376.

(6) Nilsson, L.; Halle, B. *Proc. Natl. Acad. Sci. U.S.A.* **2005**, *102*, 13867.

(7) Pal, S.; Maiti, P. K.; Bagchi, B.; Hynes, J. T. *J. Phys. Chem. B* **2006**, *110*, 26396.

(8) Sen, S.; Andreatta, D.; Ponomarev, S. Y.; Beveridge, D. L.; Berg, M. A. *J. Am. Chem. Soc.* **2009**, *131*, 1724.

(9) Thompson, W. H. *J. Chem. Phys.* **2004**, *120*, 8125.

(10) Furse, K. E.; Lindquist, B. A.; Corcelli, S. A. *J. Phys. Chem. B* **2008**, *112*, 3231.

(11) Lesch, H.; Schlichter, J.; Friedrich, J.; Vanderkooi, J. M. *Biophys. J.* **2004**, *86*, 467.

(12) Muino, P. L.; Callis, P. R. *J. Chem. Phys.* **1994**, *100*, 4093.

(13) Roux, B.; Simonson, T. *Biophys. Chem.* **1999**, *78*, 1.

(14) Sagui, C.; Darden, T. A. *Annu. Rev. Biophys. Biomol. Struct.* **1999**, *28*, 155.

(15) Tobias, D. J. *Curr. Opin. Struct. Biol.* **2001**, *11*, 253.

(16) Darden, T.; York, D.; Pedersen, L. *J. Chem. Phys.* **1993**, *98*, 10089.

(17) Essmann, U.; Perera, L.; Berkowitz, M. L.; Darden, T.; Lee, H.; Pedersen, L. G. *J. Chem. Phys.* **1995**, *103*, 8577.

(18) Ewald, P. P. *Ann. Phys.* **1921**, *64*, 253.

(19) Onsager, L. *J. Am. Chem. Soc.* **1936**, *58*, 1486.

(20) Born, M. *Z. Phys.* **1920**, *1*, 45.

(21) Grossfield, A.; Sachs, J.; Woolf, T. B. *Proteins* **2000**, *41*, 211.

(22) Rokhlin, V. *J. Comput. Phys.* **1985**, *60*, 187.

(23) Ladd, A. J. C. *Mol. Phys.* **1977**, *33*, 1039.

(24) Ladd, A. J. C. *Mol. Phys.* **1978**, *36*, 463.

(25) Neumann, M. *Mol. Phys.* **1987**, *60*, 225.

(26) Neumann, M.; Steinhauser, O.; Pawley, G. S. *Mol. Phys.* **1984**, *52*, 97.

(27) Ladanyi, B. M.; Stratt, R. M. *J. Phys. Chem.* **1995**, *99*, 2502.

(28) Wolf, D.; Keblinski, P.; Phillpot, S. R.; Eggebrecht, J. *J. Chem. Phys.* **1999**, *110*, 8254.

(29) Fennell, C. J.; Gezelter, J. D. *J. Chem. Phys.* **2006**, *124*, 234104.

(30) Zahn, D.; Schilling, B.; Kast, S. M. *J. Phys. Chem. B* **2002**, *106*, 10725.

(31) Pal, S. K.; Zhao, L. A.; Zewail, A. H. *Proc. Natl. Acad. Sci. U.S.A.* **2003**, *100*, 8113.

(32) Andreatta, D.; Lustres, J. L. P.; Kovalenko, S. A.; Ernsting, N. P.; Murphy, C. J.; Coleman, R. S.; Berg, M. A. *J. Am. Chem. Soc.* **2005**, *127*, 7270.

(33) Andreatta, D.; Sen, S.; Lustres, J. L. P.; Kovalenko, S. A.; Ernsting, N. P.; Murphy, C. J.; Coleman, R. S.; Berg, M. A. *J. Am. Chem. Soc.* **2006**, *128*, 6885.

(34) Berg, M. A.; Coleman, R. S.; Murphy, C. J. *Phys. Chem. Chem. Phys.* **2008**, *10*, 1229.

(35) Brauns, E. B.; Madaras, M. L.; Coleman, R. S.; Murphy, C. J.; Berg, M. A. *J. Am. Chem. Soc.* **1999**, *121*, 11644.

(36) Brauns, E. B.; Madaras, M. L.; Coleman, R. S.; Murphy, C. J.; Berg, M. A. *Phys. Rev. Lett.* **2002**, *88*, 158101.

(37) Brauns, E. B.; Murphy, C. J.; Berg, M. A. *J. Am. Chem. Soc.* **1998**, *120*, 2449.

(38) Coleman, R. S.; Berg, M. A.; Murphy, C. J. *Tetrahedron* **2007**, *63*, 3450.

(39) Gearheart, L. A.; Somoza, M. M.; Rivers, W. E.; Murphy, C. J.; Coleman, R. S.; Berg, M. A. *J. Am. Chem. Soc.* **2003**, *125*, 11812.

(40) Sen, S.; Gearheart, L. A.; Rivers, E.; Liu, H.; Coleman, R. S.; Murphy, C. J.; Berg, M. A. *J. Phys. Chem. B* **2006**, *110*, 13248.

(41) Sen, S.; Paraggio, N. A.; Gearheart, L. A.; Connor, E. E.; Issa, A.; Coleman, R. S.; Wilson, D. M.; Wyatt, M. D.; Berg, M. A. *Biophys. J.* **2005**, *89*, 4129.

(42) Somoza, M. M.; Andreatta, D.; Murphy, C. J.; Coleman, R. S.; Berg, M. A. *Nucleic Acids Res.* **2004**, *32*, 2494.

(43) Beck, D. A. C.; Armen, R. S.; Daggett, V. *Biochemistry* **2005**, *44*, 609.

(44) Feller, S. E.; Pastor, R. W.; Rojnuckarin, A.; Bogusz, S.; Brooks, B. R. *J. Phys. Chem.* **1996**, *100*, 17011.

(45) Hunenberger, P. H.; McCammon, J. A. *J. Chem. Phys.* **1999**, *110*, 1856.

(46) Weber, W.; Hunenberger, P. H.; McCammon, J. A. *J. Phys. Chem. B* **2000**, *104*, 3668.

(47) Lins, R. D.; Rothlisberger, U. *J. Chem. Theory Comput.* **2006**, *2*, 246.

(48) Monticelli, L.; Simoes, C.; Belvisi, L.; Colombo, G. *J. Phys.: Condens. Matter* **2006**, *18*, S329.

(49) Carter, E. A.; Hynes, J. T. *J. Chem. Phys.* **1991**, *94*, 5961.

(50) Laird, B. B.; Thompson, W. H. *J. Chem. Phys.* **2007**, *126*, 211104.

(51) Biswas, R.; Bagchi, B. *J. Phys. Chem. A* **1999**, *103*, 2495.

(52) Friedman, H. L.; Raineri, F. O.; Hirata, F.; Perng, B. C. *J. Stat. Phys.* **1995**, *78*, 239.

(53) Friedman, H. L.; Raineri, F. O.; Perng, B. C. *J. Mol. Liq.* **1995**, *7*, 65–6.

(54) Ingrosso, F.; Ladanyi, B. M. *J. Phys. Chem. B* **2006**, *110*, 10120.

(55) Ingrosso, F.; Ladanyi, B. M.; Mennucci, B.; Elola, M. D.; Tomasi, J. *J. Phys. Chem. B* **2005**, *109*, 3553.

(56) Ingrosso, F.; Tani, A.; Tomasi, J. *J. Mol. Liq.* **2005**, *117*, 85.

(57) Ishida, T.; Hirata, F.; Kato, S. *J. Chem. Phys.* **1999**, *110*, 11423.

(58) Kumar, P. V.; Maroncelli, M. *J. Chem. Phys.* **1995**, *103*, 3038.

(59) Ladanyi, B. M.; Klein, S. *J. Chem. Phys.* **1996**, *105*, 1552.

(60) Ladanyi, B. M.; Maroncelli, M. *J. Chem. Phys.* **1998**, *109*, 3204.

(61) Ladanyi, B. M.; Perng, B. C. *J. Phys. Chem. A* **2002**, *106*, 6922.

(62) Ladanyi, B. M.; Stratt, R. M. *J. Phys. Chem.* **1996**, *100*, 1266.

(63) Lobaugh, J.; Rossky, P. J. *J. Phys. Chem. A* **1999**, *103*, 9432.

(64) Maroncelli, M. *J. Chem. Phys.* **1991**, *94*, 2084.

(65) Nishiyama, K.; Yamaguchi, T.; Hirata, F.; Okada, T. *Pure Appl. Chem.* **2004**, *76*, 71.

(66) Raineri, F. O.; Perng, B. C.; Friedman, H. L. *Chem. Phys.* **1994**, *183*, 187.

(67) Roy, S.; Komath, S.; Bagchi, B. *J. Chem. Phys.* **1993**, *99*, 3139.

(68) Sudholt, W.; Staib, A.; Sobolewski, A. L.; Domcke, W. *Phys. Chem. Chem. Phys.* **2000**, *2*, 4341.

(69) Wang, J. M.; Cieplak, P.; Kollman, P. A. *J. Comput. Chem.* **2000**, *21*, 1049.

(70) Becke, A. D. *J. Chem. Phys.* **1993**, *98*, 5648.

(71) Lee, C. T.; Yang, W. T.; Parr, R. G. *Phys. Rev. B: Condens. Matter Mater. Phys.* **1988**, *37*, 785.

(72) Miehlich, B.; Savin, A.; Stoll, H.; Preuss, H. *Chem. Phys. Lett.* **1989**, *157*, 200.

(73) Cave, R. J.; Castner, E. W. *J. Phys. Chem. A* **2002**, *106*, 12117.

(74) Bayly, C. I.; Cieplak, P.; Cornell, W. D.; Kollman, P. A. *J. Phys. Chem.* **1993**, *97*, 10269.

(75) Ravi, M.; Soujanya, T.; Samanta, A.; Radhakrishnan, T. P. *J. Chem. Soc., Faraday Trans.* **1995**, *91*, 2739.

(76) Samanta, A.; Fessenden, R. W. *J. Phys. Chem. A* **2000**, *104*, 8577.

(77) Ladinig, M.; Leupin, W.; Meuwly, M.; Respondek, M.; Wirz, J.; Zoete, V. *Helv. Chim. Acta* **2005**, *88*, 53.

(78) Case, D. A.; Darden, T. A.; Cheatham, T. E.; Simmerling, C. L.; Wang, J.; Duke, R. E.; Luo, R.; Merz, K. M.; Pearlman, D. A.; Crowley, M.; Walker, R. C.; Zhang, W. ; Wang, B.; Hayik, S.; Roitberg, A.; Seabra, G.; Wong, K. F.; Paesani, F.; Wu, X.; Brozell, S.; Tsui, V.; Gohlke, H.; Yang, L.; Tan, C.; Mongan, J.; Hornak, V.; Cui, G.; Beroza, P.; Mathews, D. H.; Schafmeister, C.; Ross, W. S.; Kollman, P. A. *AMBER 9*; University of California: San Francisco, CA; 2006.

(79) Berendsen, H. J. C.; Grigera, J. R.; Straatsma, T. P. *J. Phys. Chem.* **1987**, *91*, 6269.

(80) Ryckaert, J. P.; Ciccotti, G.; Berendsen, H. J. C. *J. Comput. Phys.* **1977**, *23*, 327.

(81) Stratt, R. M.; Maroncelli, M. *J. Phys. Chem.* **1996**, *100*, 12981.

(82) Lustres, J. L. N.; Kovalenko, S. A.; Mosquera, M.; Senyushkina, T.; Flasche, W.; Ernsting, N. P. *Angew. Chem., Int. Ed.* **2005**, *44*, 5635.

(83) Karunakaran, V.; Pfaffe, M.; Ioffe, I.; Senyushkina, T.; Kovalenko, S. A.; Mahrwald, R.; Fartzdinov, V.; Sklenar, H.; Ernsting, N. P. *J. Phys. Chem. A* **2008**, *112*, 4294.

(84) Jimenez, R.; Fleming, G. R.; Kumar, P. V.; Maroncelli, M. *Nature* **1994**, *369*, 471.

CT9001416